This paper was presented at the 12th Annual Conference of the Society for Structural Integrity and Life 'Prof. Dr Stojan Sedmak' (DIVK12) November 17-19, 2024, Belgrade, Serbia

*Alfido Marchandi Faizatama[1,2], Nurman Firdaus[3], Ristiyanto Adiputra[3**], Aditya Rio Prabowo[1*], Buruhan Haji Shame[4], Martin Jurkovič[5], Andan Sigit Purwoko[3], Amar Makruf Tinulad Fil Ardli[6]*

MOORING STRESS ANALYSIS OF OC3-HYWIND FLOATING PLATFORM WITH VARIATION ANCHOR PLACEMENT

NAPONSKA ANALIZA PRIVEZIŠTA OC3-HYWIND PLUTAJUĆE PLATFORME SA PROMENOM POLOŽAJA SIDRA

Originalni naučni rad / Original scientific paper
Rad primljen / Paper received: 1.12.2024
https://doi.org/10.69644/ivk-2025-02-0193

Adresa autora / Author's address:
[1)] Department of Mechanical Engineering, Universitas Sebelas Maret, Surakarta, Indonesia *email: aditya@ft.uns.ac.id
A.R. Prabowo https://orcid.org/0000-0001-5217-5943 ;
[2)] Laboratory of Design and Computational Mechanics, Faculty of Engineering, Universitas Sebelas Maret, Surakarta, Indonesia
[3)] Research Center for Hydrodynamic Technology, National Research and Innovation Agency, Surabaya, Indonesia
N. Firdaus https://orcid.org/0009-0005-3758-0162 ;
R. Adiputra https://orcid.org/0000-0003-3630-9432 ;
A.S. Purwoko https://orcid.org/0009-0004-8276-5791
**email: ristiyanto.adiputra@brin.go.id
[4)] The Ministry of Infrastructure, Communication and Transportation, Zanzibar, Tanzania B.H. Shame https://orcid.org/0009-0001-8554-8766
[5)] Faculty of Operation and Economics of Transport and Communication, University of Zilina, Zilina, Slovakia
M. Jurkovič https://orcid.org/0000-0001-7673-1350
[6)] Research Center for Energy Conversion and Conservation, National Research and Innovation Agency (BRIN), South Tangerang, Indonesia A.M.T. Fil Ardli https://orcid.org/0009-0007-9616-7954

Keywords
- FOWT
- spar
- boundary element method
- mooring system

Abstract

This study aims to analyse the mooring stresses on the OC3-HYWIND floating platform with variations in anchor placement. The stress distribution within the mooring system is influenced by several factors, including wind direction, the presence of sea waves, and the anchor's positioning. A series of modifications is implemented in the mooring system design to enhance the effectiveness of mooring utilisation. A numerical modelling approach, utilising ANSYS® AQWA software, is employed to analyse mooring stresses. Three mooring system variations are conducted based on previous research comparing conventional mooring systems with innovative ones. The hypothesis is that the mooring variations would mitigate external influences on the mooring lines and reduce the overall stress on the system.

Ključne reči
- plutajuće vetroturbinske platforme (FOWT)
- spar
- metoda graničnih elemenata
- sistem privezivanja

Izvod

Cilj ovog istraživanja je analiza naprezanja priveza na plutajućoj platformi OC3-HYWIND sa varijacijama u postavljanju sidra. Raspodela naprezanja unutar sistema za privez podložna je uticaju brojnih faktora, uključujući pravac vetra, prisustvo morskih talasa i pozicioniranje sidra. Kako bi se povećala efikasnost korišćenja priveziša, u dizajnu sistema priveziša uveden je niz modifikacija. Pristup numeričkog modeliranja koji koristi softver ANSYS® AQWA korišćen je za analizu napona privezivanja. Proces modeliranja podrazumeva izradu matematičkih modela strukture platforme i sistema privezivanja. Sprovedene su tri varijacije sistema privezivanja od kojih su dve zasnovane na prethodnim istraživanjima, upoređujući konvencionalne sa inovativnim sistemima za privez.

INTRODUCTION

Floating offshore wind turbines (FOWTs) represent a promising technology for capturing wind energy in deep oceans, with the global floating wind market anticipated to attain 18.9 GW by 2030, /1/. The dynamic behaviour of FOWTs poses distinct problems, especially regarding platform stability and mooring system design, /2/. The OC3-Hywind spar platform, weighing 7,466,000 kg and with a draft of 120 m, has been extensively analysed as a benchmark model for floating offshore wind turbines /3/, but optimisation of its mooring configuration remains a prominent research focus.

Recent research has explored various mooring configurations to improve the motion performance of spar-type FOWTs. Ma et al. /4/ introduced a novel mooring system using fairleads positioned at varying depths (10 and 120 m), achieving notable decreases in surge (38.57 %) and pitch (20.64 %) motions relative to traditional designs with fairleads at a depth of 70 m. Building upon previous research, our paper presents a novel 'variative mooring' configuration for the OC3-Hywind platform, highlighting the impact of modifications to anchor placement.

Mooring systems are essential for preserving the location and stability of FOWTs while reducing platform movement /5/. The design of these systems must reconcile several elements, including environmental stresses, platform dynamics, and installation expenses, /6/. The OC3-Hywind platform often employs three mooring lines, each measuring

0.09 m in diameter and with an unstretched length of 902.2 m, /3/. Prior studies have examined multiple facets of FOWT mooring systems, encompassing line materials, pretension levels, /7/, and fairlead placements /8/.

Positioning of anchors in mooring systems substantially affects overall performance and load distribution /9/. Traditional designs typically employ symmetric anchor configurations with a radius of 853.87 m from the platform centre line /3/, although there is increasing interest in investigating asymmetric and optimised architecture to improve system performance /10/. This study aims to enhance existing knowledge by investigating the mooring stress characteristics of the OC3-Hywind platform under various anchor placement scenarios, with a radius ranging from 800 to 900 m.

Numerical simulation techniques, such as ANSYS® AQWA, are essential for examining the intricate coupled dynamics of FOWTs and their mooring systems /11/. Offshore structures require rigorous technical supervision and safety standards for equipment integrity and reliability in harsh marine conditions and prior structural performance diagnostics for structural revitalisation /12, 13/. These technologies allow researchers to assess different design configurations and environmental variables without incurring the expenses of actual trials /14/. The construction and renovation of efficient structural installations in the energy sector can increase industrial productivity, which in turn contributes to sustainable economic growth /15/. This study utilizes ANSYS® AQWA to simulate the OC3-Hywind platform and proposes a variable mooring configuration which accounts for wave heights of up to 6 m and wind speeds up to 11.4 m/s.

Through the investigation of mooring stresses under various anchor placements and system mooring configurations, these simulations reveal potential optimisations to improve the overall performance of the OC3-Hywind platform. This research enhances the development of FOWT designs and improves the feasibility of floating offshore wind energy, potentially reducing the levelized cost of energy (LCOE) by as much as 15 % relative to seabed-based offshore wind /16, 17/, where environmental conditions are specified.

Table 1. Summarised reference of milestone study.

Authors	Title	Experiment	Parameter
Chen et al. /18/	Experimental study on dynamic responses of a spar-type floating offshore wind turbine	Experiment in the tank test	Scaling model Environmental condition Measuring point
Utsunomiya et al. /19/	Experimental validation for motion of a spat type floating offshore wind turbine using 1/22.5 scale model	Experiment in the tank test	Scaling model Regular wave Irregular wave
Liu and Yu /20/	Dynamic response of SPAR-type floating offshore wind turbine under wave group scenarios	Numerical	Wave elevation Wind speed Catenary mooring tensions
Benassai et al. /21/	Optimization of mooring system for floating offshore wind turbines	Numerical	Scaling model Environmental condition Mooring system and type Static and dynamic load
Ma et al. /4/	Research on motion inhibition method using an innovative type of mooring system for spar floating offshore wind turbine	Numerical (BEM, ANSYS AQWA)	Mooring lines configurations (conventional and innovative) Frequency analysis Time domain analysis
Xu and Day /22/	Experiment investigation on dynamic responses of a spar-type offshore floating wind turbine and its mooring system behaviour	Experiment in the tank test	Scaling model Regular and irregular wave Mooring tension and motion
Jeon et al. /23/	Dynamic response of floating substructure of spar-type offshore wind turbine with catenary mooring cables	Numerical (BEM-FEM ANSYS AQWA)	Length of mooring cable Position of mooring cable to spar
Chen et al. /24/	Dynamic response and mooring optimization of spar-type substructure under combined action of wind, wave, and current	Numerical (ANSYS AQWA)	Scaling model (1:8) Wave condition Catenary mooring line
Li and Choung /25/	Fatigue damage analysis for a floating offshore wind turbine mooring line using the artificial neural network approach	Numerical (ANSYS AQWA)	Catenary mooring Random wave
Kamal et al. /26/	Experimental Investigation on the dynamic characteristics of a spar-type offshore wind turbine under irregular waves	Experimental in a wave tank and numerical (ANSYS AQWA)	Scaling model Irregular wave Catenary mooring Low wave frequency

METHODOLOGY

Optimisation of mooring system casing configurations is of paramount importance for the minimisation of stress force and the assurance of the platform's capacity to withstand external environmental loads. The Boundary Element Method (BEM) is crucial for analysing the hydrodynamic forces acting on the platform and its components, providing valuable insights into its motion response and load distribution. By optimising both the mooring system and understanding hydrodynamic interactions through the BEM, a more efficient and resilient spar platform design that can withstand offshore conditions can be achieved.

Case configuration

The study employs benchmarking and parametric analyses to assess hydrodynamic loads on novel moorings. A panel convergence procedure is conducted to validate the analysis procedure. A comparative analysis is conducted between the OC3 Floater Spar and conventional and innovative mooring systems. The number of panels used ranges from 1285 to 6232. The findings demonstrate a correlation between panel number and key parameters such as radiation damping and added mass in surge, heave, pitch, and steady drift motions.

Spar model for FOWT

This study utilises the OC3 Hywind floating platform as a case study to examine the advancements in floating wind energy technology. The Hywind OC3 float is designed with a low centre of gravity, enabling the deployment of wind turbines in areas with higher wind resource potential. This design mitigates environmental impact and can withstand harsh sea conditions. The parameters and dimensions of the platform spar are presented in Table 2 and illustrated in Fig. 1, /27/.

Table 2. Parameter of platform spar OC3-Hywind.

Items	Unit	Value
Mass	kg	7466000
Centre of gravity	m	(0, 0, -89.9)
Radius of gyration (R_X, R_{YY}, R_{ZZ})	m	(23.8, 23.8, 4.69)
Draft	m	120

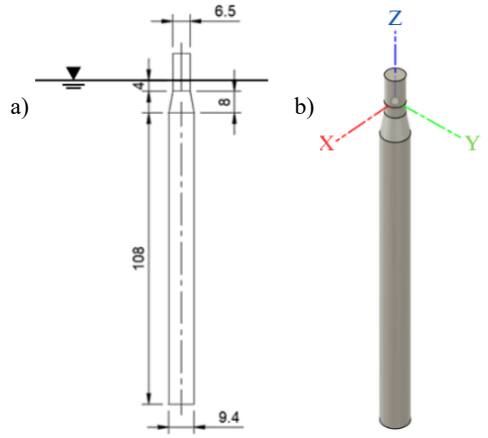

Figure 1. a) Spar OC3-Hywind dimensions; b) reference coordinate system.

Mooring design

It is imperative that offshore mooring be employed to maintain structural buoyancy and ensure safe operation. The static catenary configuration of a mooring line can be expressed through an equation that combines several factors, including water depth, the wet weight of the mooring line per unit length, the horizontal tension exerted on the mooring line at the fairlead, and the length of the suspended mooring line. The catenary profile generates geometric stiffness due to the weight of the mooring line, and the recovery strength of the catenary system is significantly affected by this weight. A schematic of a catenary-type mooring line design is presented in Fig. 2. The properties of the line can be considered to optimise the system's stability and efficiency.

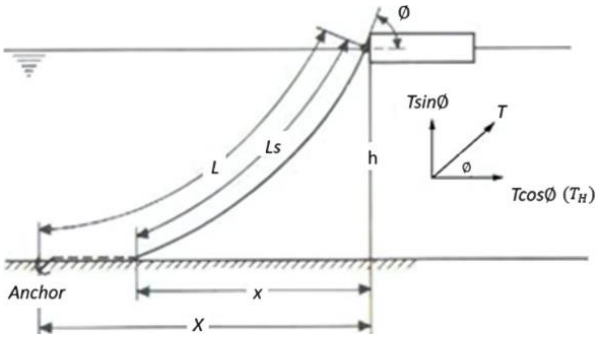

Figure 2. Schematic of mooring line, /28/.

In the absence of hydrodynamic loads and with the assumption of a single material in the elastic mooring line, the static catenary shape of the suspended line can be expressed as given in Eq.(1). The following equation can be used to calculate the variables required to determine the static catenary shape of a suspended line, assuming a single material and neglecting the hydrodynamic loads, /29/.

$$L_s = h\sqrt{2\frac{T_H}{\omega h}+1}\ , \tag{1}$$

where: h is water depth in metres; ω is mooring line wet weight per unit length in tonnes per metre; T_H is the applied horizontal load to the mooring line at the fairlead in tonnes; and L_s is the length of the suspended mooring line in metres. The horizontal distance x between the fairlead and the touchdown points of the mooring line position on the seabed can be expressed as, /29/,

$$x = \frac{T_H}{\omega}\cosh^{-1}\left(2\frac{\omega h}{T_H}+1\right). \tag{2}$$

The distance between the anchor and the line can be determined through the application of fundamental geometric principles as in the following equation, /29/,

$$X = h\sqrt{2\frac{T_H}{\omega}+1}+\frac{T_H}{\omega}\cosh^{-1}\left(\frac{\omega h}{T_H}+1\right). \tag{3}$$

To obtain the surge restoring line force, isolating and deriving T_H is necessary. The catenary profile generates geometric stiffness caused by the weight of the mooring line. The recovery force of the catenary system is highly dependent on the weight of the mooring line, as can be observed in the following equation, /29/,

$$k_{11} = \frac{\partial T_H}{\partial x} = \omega\left[\frac{-2}{2\frac{\omega h}{T_H}+1}+\cosh^{-1}\left(\frac{\omega h}{T_H}+1\right)\right]^{-1}. \tag{4}$$

The utilisation of a mooring system can significantly improve the stiffness of a spar platform, reducing the influence of currents, wind, and waves, which can induce dynamic movements like surge, sway, heave, roll, pitch, and yaw, thereby enhancing stability and efficiency, /30/.

The alignment of all mooring lines at the same horizontal distance, a conventional system, can result in increased motion and reduced stability when subjected to dynamic environmental conditions. In contrast, this novel technology addresses both horizontal and pitch motions, thereby enhancing the performance of the FOWT. The data demonstrate a reduction in the mean, maximal value, and standard deviation of pitch motion by 17.87 %, 20.64 %, and 18.37 %,

respectively, compared to the conventional system. The data obtained facilitate the optimisation of the mooring system through modification, reducing the applied tension force and emphasizing stability, especially for horizontal and pitch motion. Relevant parameters related to the mooring line are shown in Table 3 and illustrated in Figs. 3 and 4.

Table 3. Parameters of mooring line.

Items	Unit	Value		
Type		Conventional	Innovative	Variative
Mass	kg/m	130.5	130.5	130.5
Diameter	m	85	85	85
Break load	MN	7.37	7.37	7.37
Extensional stiffness	MN	539	539	539
Depth of anchor	m	320	320	320
Length	m	950	1145/650	990/505
Horizontal span	m	880.7	1063/590.5	903.5/442.875
Depth of fairleads	m	70	10/120	10/120
Angle between mooring 1 & 2	°	15	15	22.5

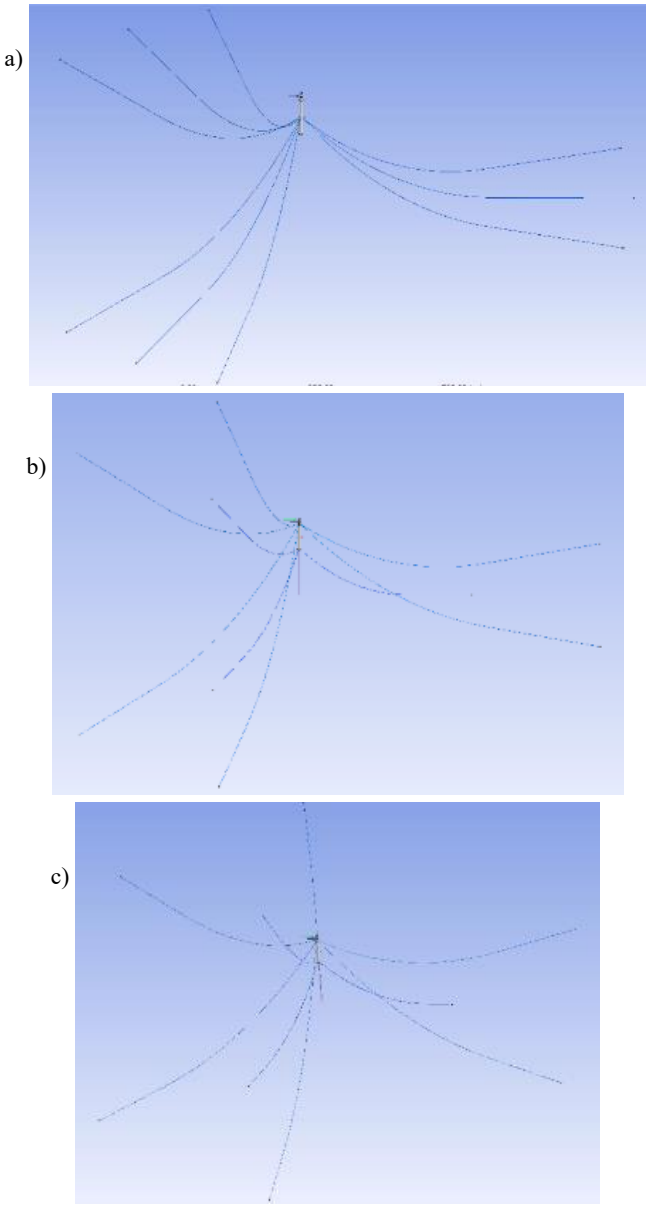

Figure 3. Three types of mooring systems: a) conventional; b) innovative; c) variative.

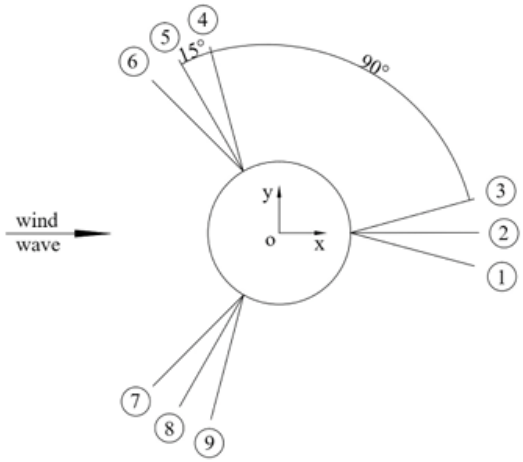

Figure 4. Top view layout mooring system, /4/.

Environment condition

A series of simulations are conducted utilising a range of mooring systems in the Timor Sea region /31/ under conditions devoid of meteorological activity. The environmental parameters employed reflected a relatively moderate hydrodynamic situation. The Timor Sea is renowned for its stable marine conditions outside the hurricane season, which permit the utilisation of environmental parameters such as low to moderate wave height, moderate wind speed, and consistent ocean currents. Table 4 presents the environmental conditions in the area. This simulation assesses the mooring system's functionality and the platform's hydrodynamic response under typical operational conditions in the specified area, where external disturbances are minimal. Such studies are essential for understanding the performance of FOWT spar under typical operating conditions, particularly in maintaining structural integrity and reducing unwanted motions without significant wave or wind influences while ensuring the reliability of the resulting renewable energy system.

Table 4. Parameters of environment condition Timor Sea /32/.

Items	Symbol	Unit	Value
Significant wave height	H_s	m	4.8
Wave period	T_p	s	11.5
	T_z	s	8.3
Gamma	γ		1
Wind velocity	V_{wind}	m/s	16.6
Current	$V_{current}$	m/s	1.1

BOUNDARY ELEMENT METHOD

Potential flow equations can be efficiently solved through the boundary element method (BEM) to model the response of structures to the effects of waves, currents, and wind. This method necessitates only the surface of the structure to be discretised (panel discretisation) which markedly reduces the computational complexity. ANSYS® AQWA employs the BEM to calculate the hydrodynamic forces acting on the model. Furthermore, BEM is also used for modelling and calculating radiation damping, added mass, and steady drift, which are essential components in dynamic response analysis. This method allows for the evaluation of structure motion under irregular wave conditions and the analysis of mooring stresses generated by the interaction of waves with the mooring systems.

Airy theory wave

In the context of wave modelling, the underlying assumptions typically encompass incompressibility. The assumptions, as mentioned earlier, include those on compressible flow, irrotational flow, and inviscid fluid, /33/. The continuity of incompressible flow for three-dimensional bodies is as follows:

$$\frac{\partial u}{\partial x}+\frac{\partial v}{\partial y}+\frac{\partial w}{\partial z}=0\cdot \tag{5}$$

The velocity component for the *x*-direction is represented by variable *u*. The velocity component for the *y*-direction is designated as *v*. In contrast, the velocity component for the z-direction is designated as *w*. For an irrational flow, the vorticity (defined herein as the velocity curve) becomes zero, as expressed by the following equation:

$$\omega_x=\frac{1}{2}\left[\frac{\partial w}{\partial y}-\frac{\partial v}{\partial z}\right]=0\ , \tag{6}$$

$$\omega_y=\frac{1}{2}\left[\frac{\partial u}{\partial z}-\frac{\partial w}{\partial x}\right]=0\ , \tag{7}$$

$$\omega_z=\frac{1}{2}\left[\frac{\partial v}{\partial z}-\frac{\partial u}{\partial y}\right]=0\ . \tag{8}$$

In this context, the rotational components along the *x*, *y*, and *z* directions are represented by ω_x, ω_y, and ω_z, in respect. The velocity potential, a function of ϕ, can describe the wave flow analysis around the spar-type platform and the hydrodynamic forces. The variables *x*, *y*, and *z* are defined as follows:

$$u=\frac{\partial\phi}{\partial x}\ , \tag{9}$$

$$v=\frac{\partial\phi}{\partial y}\ , \tag{10}$$

$$w=\frac{\partial\phi}{\partial z}\ . \tag{11}$$

The wave velocity potential can be expressed as /34/:

$$\phi(x,y,t)=\frac{H}{2}\frac{g}{\omega}\frac{\cosh(k(z+d))}{\cosh(kd)}\sin(kx-\omega t)\ , \tag{12}$$

where: *H* and *k* can be expressed as wave height and wave number; while ω indicates angular frequency. With the velocity potential result, the fluid velocity (*u*, *w*) can be determined, but when considering flat waves, the velocity component *v* in the *y* direction is 0. The detailed expressions are as follows:

- horizontal velocity component *u* in the *x* direction

$$u=\frac{\partial\phi}{\partial x}=\frac{H}{2}\omega\frac{\cosh(k(z+d))}{\sinh(kd)}\cos(kx-\omega t)\ , \tag{13}$$

- vertical velocity component *w* in the *z* direction

$$w=\frac{\partial\phi}{\partial z}=\frac{H}{2}\omega\frac{\sinh(k(z+d))}{\sinh(kd)}\sin(kx-\omega t)\cdot \tag{14}$$

The velocity component in the *y*-direction of *v* is 0 due to the assumption of flat waves

$$v=0\ . \tag{15}$$

The result of the fluid velocity calculation is used in the Bernoulli equation to determine how much pressure occurs in the structure, /35/.

$$p+\frac{1}{2}\rho v^2+\rho gh=C\cdot \tag{16}$$

- Dynamic pressure

$$P_d=\frac{1}{2}\rho u^2\ , \tag{17}$$

$$P_d=\frac{1}{2}\rho\left(\frac{H}{2}\omega\frac{\cosh(k(z+d))}{\sinh(kd)}\cos(kx-\omega t)\right)^2\ , \tag{18}$$

- Total pressure

$$P_d+P_a=P\ , \tag{19}$$

$$P=P_a+\frac{1}{2}\rho\left(\frac{H}{2}\omega\frac{\cosh(k(z+d))}{\cosh(kd)}\cos(kx-\omega t)\right)^2\ , \tag{20}$$

where: *p* is pressure; ρ is density of fluid; *v* is fluid velocity; *g* is acceleration of gravity; and *h* is surface elevation. For a free surface we can ignore the elevation *h*. This dynamic and total pressure affect waves that occur and the forces the structure receives.

Equation of motion

Modelling in ANSYS® AQWA is a combination of panels and Morison elements. The following equations give structural equations of motion with frequency-dependent coefficients:

$$[F'_{jm}]=[x_{jm}][-\omega^2(M_s+M'_a)-i\omega C'+K'_h+K_a]\cdot \tag{21}$$

Matrices M_s and M_a' correspond to total structural mass and total added mass, respectively, due to the Morison element and diffraction panels. The coefficient *C* denotes the hydrodynamic damping matrix associated with diffraction panels. K_h and K_a are the assembled hydrostatic stiffness and the additional structural stiffness, respectively. The term F_{jm}' signifies the collective Froud-Krylov and diffracting forces and moments, where variable '*m*' represents the structure and '*j*' refers to the motion mode (6 DOF).

To model the mooring line, the Morison element is used, subjected to hydrodynamic inertia and external structural loads /36/, where diffraction effects do not dominate the hydrodynamic force on the mooring line. The motion equation for each cable element can be written as follows:

$$\frac{\partial\vec{T}}{\partial s_e}+\frac{\partial\vec{V}}{\partial s_e}+\vec{W}+\vec{F}_h=m\frac{\partial^2\vec{R}}{\partial t^2}\ , \tag{22}$$

$$\frac{\partial\vec{M}}{\partial s_e}+\frac{\partial\vec{R}}{\partial s_e}+\vec{V}=-\vec{q}\ . \tag{23}$$

Values of $\vec{R}$, $\vec{T}$, $\vec{M}$, and $\vec{V}$ are determined at the initial node of the element and represent the position, tensile force, bending moment, and shear force vectors. Additionally, $\vec{F}_h$, $\vec{q}$, *m*, and $\vec{W}$ are determined per unit length and represent external hydrodynamic loading, distributed moment, structural mass, and element weight.

Frequency domain analysis

According to the theory of three-dimensional potential flows, the diffraction and radiation potential can be calculated by resolving the boundary integral equation that meets the specified conditions. The first-order hydrodynamic force is represented by F_j:

$$F_j e^{-i\omega t}=[-i\omega\rho\textstyle\int_{s_0}\phi(\vec{X})n_j dS]e^{-i\omega t}\ , \tag{24}$$

where: ω is wave frequency; ρ is fluid density; s_0 is mean wetted surface of body; ϕ is velocity potential, $\vec{X}=(X, Y, Z)$

is the location of a point on the submerged body surface; n_j is unit normal vector of the body surface pointing outwards; $j = 1…6$ represents 6 DOF.

The additional mass and radiation damping coefficients can be obtained by:

$$A_{jk}(\omega)+i\frac{B_{jk}(\omega)}{\omega}=-i\frac{\rho}{\omega}\int_{s_0}\phi_{rk}(\vec{X})n_j dS=F_{rjk}\,, \quad (25)$$

where: A_{jk} and B_{jk} are respectively added mass and damping coefficients in frequency domain; F_{rjk} is the radiation force induced by amplitude motion; ϕ_{rk} is the radiation potential.

Time domain coupled analysis

This analysis aims to evaluate the time-varying dynamic response of a structure to an external excitation or force. The time domain coupled motion can be obtained by solving Cummins equation:

$$(M)\ddot{X}(t)+\int_0^t \dot{X}(\tau)R(t-\tau)d\tau+C\dot{X}(t)+KX(t)=F_e(t)\,, \quad (26)$$

where: M is structural mass matrix; R is velocity impulse function; $\dot{X}$ represents velocity; C is damping matrix including radiation and auxiliary damping; K is hydrostatic recovery stiffness matrix; F_e is exciting force which includes wave load (first-order, mean drift and difference frequency wave force), and mooring system recovery force.

RESULT AND DISCUSSION

Panel convergence and benchmarking

A hydrodynamic analysis of the OC3-Hywind floating platform is conducted utilising a boundary element method. The objective of this analysis is to assess the convergence of the mesh and evaluate key hydrodynamic parameters. A comprehensive mesh convergence study utilised six-panel numbers ranging from 1258 to 6232. This study aims to identify the optimal mesh resolution for accurately predicting hydrodynamic coefficients while maintaining computational efficiency.

The mean drift force, a critical parameter for mooring system design, demonstrates a notable variation in the number of panels, particularly at lower frequencies, as illustrated in Fig. 5. As mesh resolution increases, the predicted mean drift force exhibits convergence, with the 5364 and 6232 number of panels demonstrating close agreement across the frequency range. This convergence indicates that a minimum of 5364 elements is necessary for reliable prediction of mean drift forces, which is crucial for accurately estimating the steady-state offset of the floating platform.

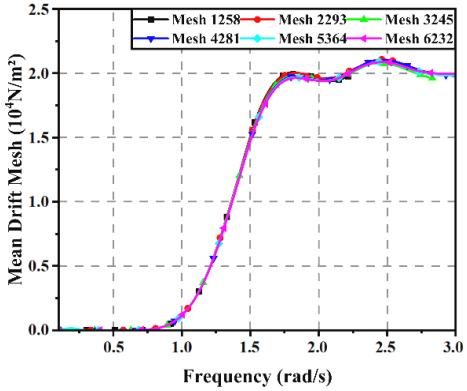

Figure 5. Mean drift mesh variation.

As illustrated in Fig. 6, the surge added mass results exhibit a discernible trend of declining values with rising frequency. This aligns with the anticipated behaviour of spar platforms. The variation in surge-added mass is more pronounced at lower frequencies, with the use of coarser meshes generally resulting in the prediction of higher values. Convergence improved markedly at higher frequencies, indicating that mesh density is significant for the analysis of low-frequency motion. As illustrated in Fig. 7, the heave-added mass exhibits a distinctive peak at approximately 0.3 rad/s, with excellent convergence across all mesh densities, particularly above 0.5 rad/s. This peak indicates the potential for a resonance frequency for heave motion which should be carefully considered in the platform's design to avoid excessive vertical motion.

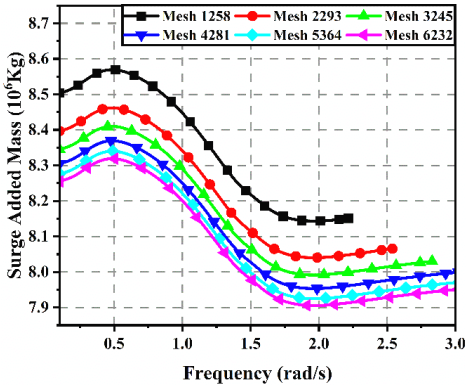

Figure 6. Surge added mass mesh variation.

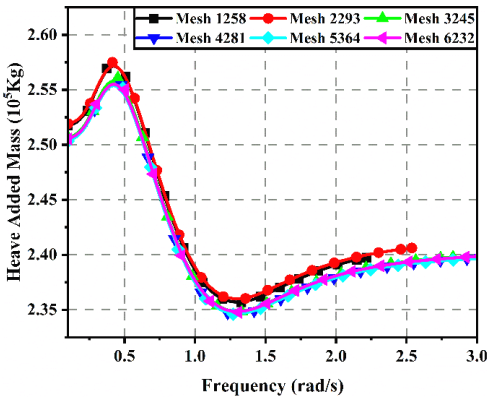

Figure 7. Heave added mass mesh variation.

Results for pitch added mass, Fig. 8, demonstrate a pattern similar to that observed for surge but with a more pronounced sensitivity to mesh density across the frequency range. The variation between mesh densities was most significant at low frequencies, emphasizing the importance of adequate mesh refinement for accurate prediction of rotational inertia effects. The convergence of pitch-added mass results suggests that a mesh with at least 4281 elements is necessary for reliable rotational motion analysis.

The radiation-damping characteristics for surge, heave, and pitch motions, as illustrated in Figs. 9, 10, and 11, exhibit excellent convergence across all mesh densities. The surge radiation damping exhibits a maximal value of approximately 1.2 rad/s, while the heave radiation damping demonstrates a maximal value of approximately 0.6 rad/s. The pitch radiation damping exhibits a broader peak, centred around 0.8 rad/s. The consistent convergence of radiation-damping

results across mesh densities indicates that even coarser mesh may be sufficient for predicting the energy dissipation characteristics of the platform.

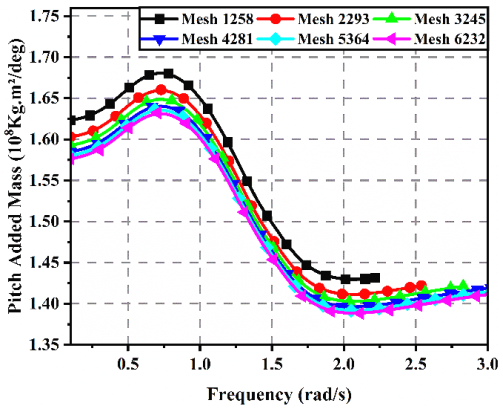

Figure 8. Pitch-added mass mesh variation.

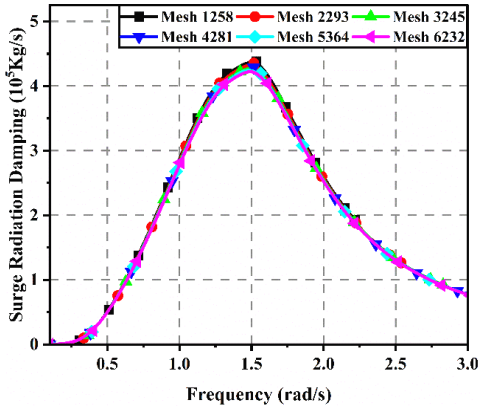

Figure 9. Surge radiation damping mesh variation.

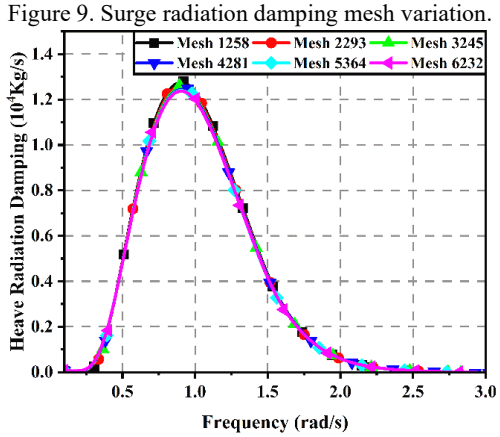

Figure 10. Heave radiation damping mesh variation.

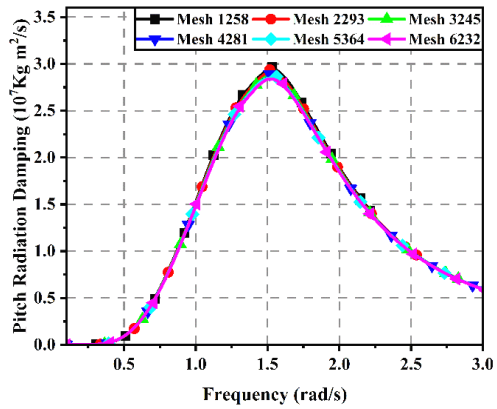

Figure 11. Pitch radiation damping mesh variation.

Results of the time-domain study, illustrated in Figs. 12-15, provide additional information that describes the platform's dynamic behaviour when subjected to simulated environmental circumstances. Figure 12 shows mooring tension at line 1 with mesh variation; Fig. 13 shows mooring tension at line 2 with mesh variation; Fig. 14 shows tension at line 4 with mesh variation; and Fig. 15 shows mooring tension at line 5 with mesh variation. Although the surge motion exhibits oscillations of around 10 m, it was the motion that displayed the most significant amplitudes. The fact that the platform is susceptible to the excitation of low-frequency waves is demonstrated by this circumstance. While the heave motion was occurring, the amplitudes were diminished and were approximately 2 m in magnitude. Another indication of the platform's resistance to rotational excitation is that pitch motion was maintained within a range of 2 degrees. This motion was maintained throughout the experiment.

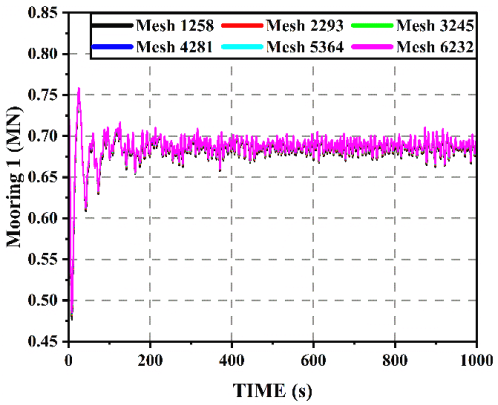

Figure 12. Mooring tension at line 1 with mesh variation.

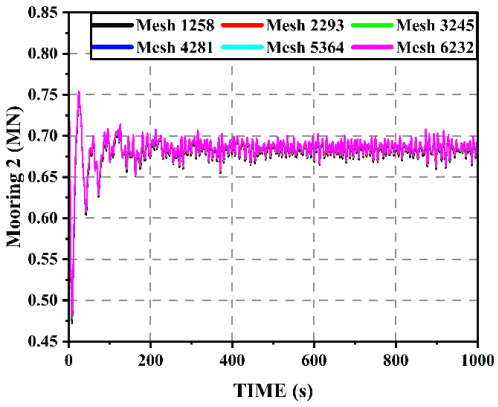

Figure 13. Mooring tension at line 2 with mesh variation.

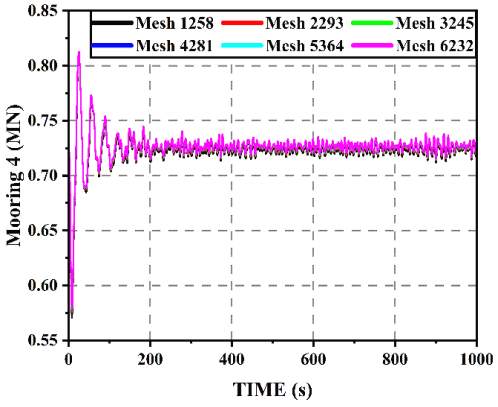

Figure 14. Mooring tension at line 4 with mesh variation.

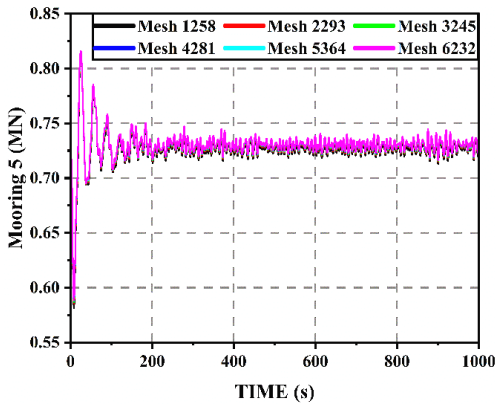

Figure 15. Mooring tension at line 5 with mesh variation.

Since findings are only gathered from a fraction of the mooring lines, this particular mooring line is provided here. As a result of the fact that some mooring lines are identical to their anchor placement, this consequence has arisen.

A comparison is made between the findings obtained with the finest mesh (6232 panels) and the benchmark data, and the results show a high degree of agreement for most of the hydrodynamic parameters. It is determined that this is the case when the findings are compared. To validate the validity of the numerical model currently applied, it is discovered that the mean drift force estimates are in good agreement with the benchmark data. This is performed to validate the credibility of the model. Particularly within the frequency range of 0.2 to 2 rad/s, relevant for ordinary ocean wave circumstances, the surge, heave, and pitch on radiation damping and additional mass display a significant connection with the benchmark data.

Comparison of the mooring system

Once the optimal number of panels for accurate hydrodynamic modelling are determined, a comprehensive mooring system comparison is conducted to evaluate its performance under simulated environmental conditions. This analysis examines mooring line tension and its effect on the operation of the turbine system. By comparing different mooring configurations, including conventional, innovative, and variative systems, the discussion highlights how they respond to external forces, emphasizing differences in stress distribution, total mooring length, and the corresponding impact on platform stability and economic viability.

Figures 16 to 21 illustrate the comparison between the mooring lines. Figure 16 shows comparison tension of mooring line 1; Fig. 17 shows comparison tension of mooring line 2; Fig. 18 shows comparison of mooring line 3; Fig. 19 shows comparison tension of mooring line 4; Fig. 20 shows comparison tension of mooring line 5; and Fig. 21 shows comparison tension of mooring line 6.

The simulation findings indicate that stresses encountered by each mooring depend on the particular method utilised. Strains are detected in moorings 1, 3, 4, and 6. Conventional systems are generally more compact. The homogeneous stress distribution across three moorings on each side results in modest stresses in conventional systems. Conversely, innovative and variative systems have merely two similar moorings on each side and one shorter mooring, leading to a diminished distribution of loads.

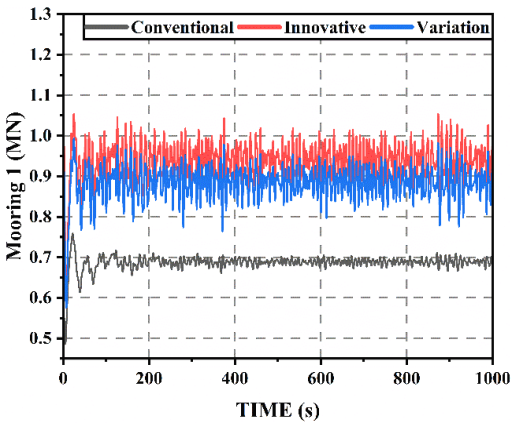

Figure 16. Comparison tension of mooring line 1.

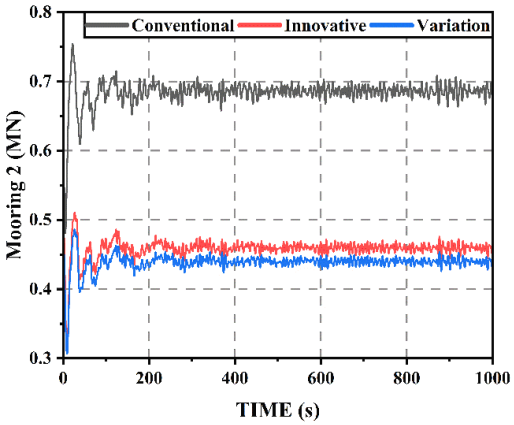

Figure 17. Comparison tension of mooring line 2.

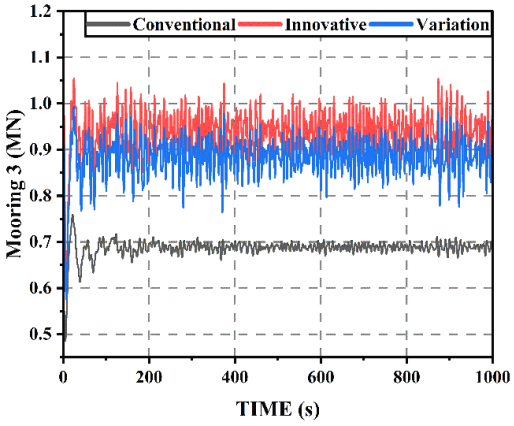

Figure 18. Comparison tension of mooring line 3.

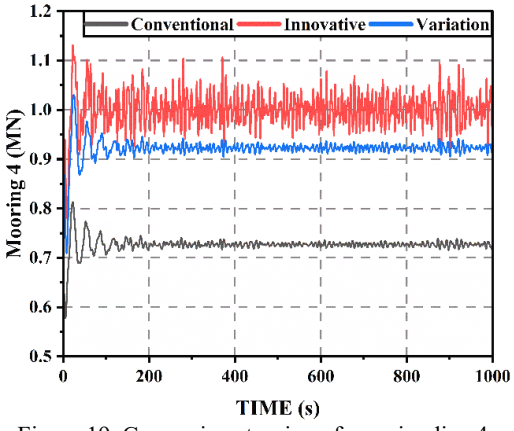

Figure 19. Comparison tension of mooring line 4.

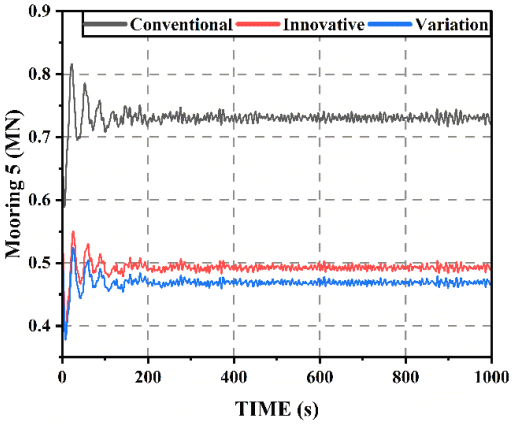

Figure 20. Comparison tension of mooring line 5.

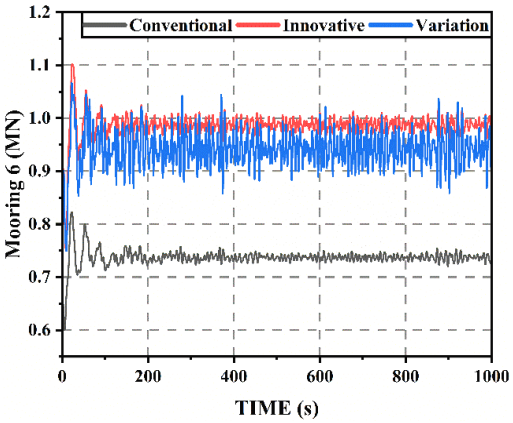

Figure 21. Comparison tension of mooring line 6.

Table 5. Mooring stress/force (MN) statistic.

Mooring line	Parameters	Conventional	Innovative	Variation
1	Max Tension	0.822	1.122	1.052
	Mean Tension	0.687	0.937	0.882
	Pre-Tension	0.482	0.57	0.573
2	Max Tension	0.819	0.584	0.552
	Mean Tension	0.684	0.458	0.438
	Pre-Tension	0.478	0.310	0.305
3	Max Tension	0.822	1.122	1.052
	Mean Tension	0.687	0.937	0.882
	Pre-Tension	0.482	0.577	0.573
4	Max Tension	0.837	1.133	1.046
	Mean Tension	0.727	1.002	0.922
	Pre-Tension	0.576	0.779	0.706
5	Max Tension	0.836	0.596	0.563
	Mean Tension	0.731	0.492	0.469
	Pre-Tension	0.587	0.388	0.376
6	Max Tension	0.839	1.122	1.070
	Mean Tension	0.737	0.988	0.943
	Pre-Tension	0.598	0.750	0.746

Each side has a shorter mooring, enhancing stress distribution across the two remaining moorings. The quantity of moorings is generally higher. From Table 5, statistics reveal that moorings 2 and 5 exhibit markedly higher tensions in the conventional system compared to the other two systems. Innovative and variative systems demonstrate minimal distinction. Stresses on each mooring in the variable system are often lower than those in the inventive system.

A new system has been developed. An augmentation of the angle and a decrease in the horizontal span within the variation system can alleviate the strains encountered by the mooring. The variative system possesses the capacity to diminish stress levels markedly. The shortened horizontal span decreases the total mooring length, reducing installation costs. Additionally, the data illustrate the escalation of tension concerning the pre-tension of each mooring.

CONCLUSIONS

Based on the results of the analyses and the conducted studies, the following conclusions can be drawn:

- The variative mooring system exhibits reduced strains compared to the innovative system; by decreasing the distance between anchor points and the platform, the overall mooring length can be minimised, minimising the tension in mooring lines. The cumulative mooring length in the innovative system is 8820 m, whereas the variative system measures 7455 m. This lowering not only alleviates tension but also improves the economic efficiency of the mooring system.
- The percentage rise in stress compared to initial stress values demonstrates that the variative system produces lesser stress rises than the innovative system. In mooring 1, the stress increase for innovative and variative systems is 54.5 % and 47.9 %, respectively. The increases for mooring 2 are 27.4 % and 24.7 %, while for mooring 4, they are 35.4 % and 34 %. Mooring 5 exhibits a stress augmentation of 20.8 % in the innovative system and 18.7 % in the variative system, while mooring 6 shows increases of 37.2 % and 32.4 %, respectively. The findings indicate that the variative system is a more effective solution for alleviating stress in mooring lines, rendering it a superior option for design.

Conventional systems exhibit an even stress distribution. In contrast, innovative and variative systems exhibit an unbalanced stress distribution, with the most significant stresses occurring at longer moorings. Variative systems offer advantages in stress reduction and mooring lengths. Furthermore, the stress rise in the variative system is lower than that of the innovative system, making it a more practical option for developing efficient and reliable mooring systems in offshore operations.

ACKNOWLEDGEMENTS

This work is supported by the RKAT Universitas Sebelas Maret - Year 2025, under the Research Scheme of 'PENGUATAN KAPASITAS GRUP RISET' (PKGR-UNS) A, with research grant/contract no. 371/UN27.22/PT.01.03/2025. The authors highly acknowledge this support.

REFERENCES

1. Jonkman, J.M., Matha, D. (2011), *Dynamics of offshore floating wind turbines-analysis of three concepts*, Wind Energy, 14(4): 557-569. doi: 10.1002/we.442
2. Butterfield, S., Musial, W., Jonkman, J., et al. (2007), *Engineering challenges for floating offshore wind turbines*, In: Copenhagen Offshore Wind Conf. 2007, NREL/CP-500-38776, National Renewable Energy Lab. (U.S.), Golden, CO., 13 p.
3. Robertson, A., et al. (2014), *Definition of the semisubmersible floating system for phase II of OC4*, Tech. Rep. NREL/TP-5000-60601, National Renewable Energy Lab. (U.S.), Golden, CO., 42 p.
4. Ma, Y., Chen, C., Fan, T., et al. (2021), *Research on motion inhibition method using an innovative type of mooring system for spar floating offshore wind turbine*, Ocean Eng. 223: 108644. doi: 10.1016/j.oceaneng.2021.108644

5. Karimirad, M., Offshore Energy Structures : For Wind Power Wave Energy and Hybrid Marine Platforms, Springer Cham, 2014. doi: 10.1007/978-3-319-12175-8
6. Bachynski, E.E., Moan, T. (2012), *Design considerations for tension leg platform wind turbines*, Mar. Struct. 29(1): 89-114. doi: 10.1016/j.marstruc.2012.09.001
7. Kwan, C.T., Bruen, F.J. (1991), *Mooring line dynamics: comparison of time domain, frequency domain, and quasi-static analyses*, In: Proc. 23rd Annual Offshore Technology Conf., Houston TX, 1991, Vol.3, Ppr OTC 6657, pp.95-108. ISBN: 978-1-61399-087-2
8. Agarwal, A.K., Jain, A.K. (2003), *Dynamic behavior of offshore spar platforms under regular sea waves*, Ocean Eng. 30(4): 487-516. doi: 10.1016/S0029-8018(02)00034-3
9. Hallowell, S.T., et al. (2018), *System reliability of floating offshore wind farms with multiline anchors*, Ocean Eng. 160: 94-104. doi: 10.1016/j.oceaneng.2018. 04.046
10. Fontana, C.M., et al. (2016), *Efficient multiline anchor systems for floating offshore wind turbines*, In: Proc. Int. Conf. on Ocean, Offshore Mech. and Arctic Eng. (OMAE2016), Busan, Korea, 2016, ASME. doi: 10.1115/ OMAE2016-54476
11. Chen, L., Basu, B. (2018), *Fatigue load estimation of a spar-type floating offshore wind turbine considering wave-current interactions*, Int. J Fatigue, 116: 421-428. doi: 10.1016/j.ijfatigue.2018.06.002
12. Maneski, T., Ignjatović, D. (2004), *Structural performance diagnostics*, Struct. Integr. Life, 4(1): 3-7.
13. Bređan, A., Kurai, J. (2001), *Requirements, practice and dilemas at technical surveillance of equipment in service*, Struct. Integr. Life, 1(1): 19-22. (in Serbian)
14. Thomsen, J.B., (2017), *Validation of a tool for the initial dynamic design of mooring systems for large floating wave energy converters*, J Mar. Sci. Eng. 5(4): 45. doi: 10.3390/jmse5040045
15. Garić, N., Kurai, J. (2001), *Renovation of destroyed equipment in pančevo oil refinery*, Struct. Integr. Life, 1(1): 13-17.
16. Lefebvre, S., Collu, M. (2012), *Preliminary design of a floating support structure for a 5 MW offshore wind turbine*, Ocean Eng. 40: 15-26. doi: 10.1016/j.oceaneng.2011.12.009
17. Fauzi, F.N., et al. (2024), *Implementation assessment of the Offshore Wind Turbine (OWT) for remote regions' electrification in Indonesia based on geographical potential and economic attractiveness*, Eng. Sci. 32: 1295. doi: 10.30919/es1295
18. Chen, J., Liu, Z., Song, Y., et al. (2022), *Experimental study on dynamic responses of a spar-type floating offshore wind turbine*, Renew. Energy, 196: 560-578. doi: 10.1016/j.renene.2022.06.149
19. Utsunomiya, T., et al. (2009), *Experimental validation for motion of a SPAR-type floating offshore wind turbine using 1/22.5 scale model*, In: Proc. Int. Conf. Offshore Mech. and Arctic Eng. (OMAE2009), Honolulu, HI, USA, pp. 951-959. doi: 10.1115/OMAE2009-79695
20. Liu, B., Yu, J. (2022), *Dynamic response of SPAR-type floating offshore wind turbine under wave group scenarios*, Energies, 15(13): 4870. doi: 10.3390/en15134870
21. Benassai, G., et al. (2015), *Optimization of mooring systems for floating offshore wind turbines*, Coast. Eng. J, 57(4): 1550021. doi: 10.1142/S057856 3415500217
22. Xu, X., Day, S. (2021), *Experimental investigation on dynamic responses of a spar-type offshore floating wind turbine and its mooring system behaviour*, Ocean Eng. 236: 109488. doi: 10.1016/j.oceaneng.2021.109488
23. Jeon, S.H., et al. (2013), *Dynamic response of floating substructure of spar-type offshore wind turbine with catenary mooring cables*, Ocean Eng. 72: 356-364. doi: 10.1016/j.oceaneng.2013.07.017
24. Chen, D., et al. (2017), *Dynamic response and mooring optimization of spar-type substructure under combined action of wind, wave, and current*, J Renew. Sustain. Energy, 9(6): 0633 07. doi: 10.1063/1.5017228
25. Li, C.B., Choung, J. (2017), *Fatigue damage analysis for a floating offshore wind turbine mooring line using the artificial neural network approach*, Ships Offshore Struct. 12(Sup. 1): S288-S295. doi: 10.1080/17445302.2016.1254522
26. Shalabe, A., et al. (2023), *Experimental investigation on the dynamic characteristics of a spar-type offshore wind turbine under irregular waves*, J Al-Azhar Univ. Eng. Sect. 18(69): 830-849. doi: 10.21608/auej.2023.219019.1388
27. Jonkman, J., Definition of the floating system for phase IV of OC3, Nat. Renewable Energy Lab., Tech. Rep. NREL/TP-500-47535, 2010. doi: 10.2172/979456
28. Huang, W.-H., Yang, R.-Y. (2021), *Water depth variation influence on the mooring line design for FOWT within shallow water region*, J Mar. Sci. Eng. 9(4): 409. doi: 10.3390/jmse9040409
29. Ma, K.-T., et al., Mooring System Engineering for Offshore Structures, Chapter 5 - Mooring Analisys, Gulf Prof. Publ., Elsevier Inc., 2019: 85-114. doi: 10.1016/B978-0-12-818551-3.00005-3
30. Campanile, A., et al. (2018), *Mooring design and selection for floating offshore wind turbines on intermediate and deep water depths*, Ocean Eng. 148: 349-360. doi: 10.1016/j.oceaneng.2017.11.043
31. RPS MetOcean Pty Ltd., Metocean Criteria Guidelines for MODU Mooring on Australia's Northwest Shelf, Tech. Note No: 100-CN-TNT-0819 Rev 0 Job No: J3081, AEP, 2016.
32. DNVGL-OS-E301, Position mooring, DNV GL AS, 2015.
33. Babarit, A., Delhommeau, G. (2015), *Theoretical and numerical aspects of the open source BEM solver NEMOH*, 11th Eur. Wave Tidal Energy Conf. (EWTEC2015), 2015, Nantes, France. https://hal.science/hal-01198800v1
34. Dean, R.G., Dalrymple, R.A., Water Wave Mechanics for Engineers and Scientists, P.LF Liu (Ed.): Advanced Series on Ocean Engineering: Vol. 2, World Scientific Publ. Co. Pte Ltd., Singapore, 1991. doi: 10.1142/1232
35. Newman, J.N., Marine Hydrodynamics, MIT Press, Cambridge, Massachusetts, 2017.
36. Ghafari, H.R., et al. (2019), *Numerical study on the hydrodynamic interaction between two floating platforms in Caspian Sea environmental conditions*, Ocean Eng. 188: 106273. doi: 10.1016/j.oceaneng.2019.106273

© 2025 The Author. Structural Integrity and Life, Published by DIVK (The Society for Structural Integrity and Life 'Prof. Dr Stojan Sedmak') (http://divk.inovacionicentar.rs/ivk/home.html). This is an open access article distributed under the terms and conditions of the Creative Commons Attribution-NonCommercial-NoDerivatives 4.0 International License